Long-term performance analysis of an HT-PEM fuel cell based micro-CHP system: Operational strategies

Behzad Najafi *, Alireza Haghighat Mamaghani, Fabio Rinaldi, Andrea Casalegno

Dipartimento di Energia, Politecnico di Milano, Via Lambruschini 4, 20156 Milano, Italy

Received 26 September 2014
Received in revised form 24 February 2015
Accepted 7 March 2015

1. Introduction

In the past few decades, interest and investment in renewable energy resources have considerably been increased. In this context, fuel cells appear to be one of the most suitable alternatives for conventional power generation systems, in both stationary and mobile applications. Amongst various types of fuel cells, Proton Exchange Membrane (PEM) fuel cells have been considered as one of the most promising types, owing to their high efficiency, high energy/power densities, low/zero emissions, long stack life, and fast response in comparison with the other types of fuel cells [1–4]. Low temperature PEM (LT-PEM) fuel cells are the most

* Corresponding author. Tel.: +39 02 2399 3840.
E-mail addresses: behzad.najafi@polimi.it (B. Najafi), alireza.haghighat@mail.polimi.it (A. Haghighat Mamaghani), fabio.rinaldi@polimi.it (F. Rinaldi), andrea.casalegno@polimi.it (A. Casalegno).

Nomenclature

Acronyms

CHP	combined heat and power
GDL	gas diffusion layer
HT-PEM	high temperature proton exchange membrane
LMTD	logarithmic mean temperature difference
LT-PEM	low temperature proton exchange membrane
MEA	membrane electrode assembly
OHM	ohmic
PBI	polybenzimidazole
PES	primary energy saving
PFSA	perfluorosulfonic acid
PrOX	preferential oxidation
SMR	steam methane reforming
WGS	water gas shift
WKO	water knock out

Symbols

E_{ID}	ideal voltage (V)
E_a	activation energy (kJ mol^{-1})
f	friction factor
ΔH_{298K}	standard enthalpy of reaction (kJ kmol^{-1})
I	current (A)
k	rate coefficient
K	equilibrium constant
LHV	low heating value (kJ kg^{-1})
$\dot{m}$	mass flow rate (kg s^{-1})
N	number of cells
Nu	Nusselt number
P_x	partial pressure of species x
P	power (kW)
Pr	Prandtl number
$\dot{Q}$	the time rate of heat transfer (kW)
r	rate of reaction (mol l^{-1} s^{-1})
R	universal gas constant (kJ kmol K^{-1})
Re	Reynolds number
T	temperature (K)
V	voltage (V)

Subscripts

A	anode
C	cathode
cogen	cogeneration
el	electrical
th	thermal

Greek symbols

η_A	anodic voltage loss
η_C	cathodic voltage loss
η_{el}	electrical efficiency
η_I	first law efficiency
η_{th}	thermal efficiency
λ_{H_2}	anodic stoichiometric ratio

well-recognized type of PEM fuel cells with low operating temperatures (around 80 °C) and Nafion-based proton exchange membrane. Numerous studies have been conducted on the application of LT-PEM fuel cell for cogeneration and trigeneration purposes [5–8].

Radulescua et al. [6] carried out an experimental and theoretical analysis on identical LT-PEM fuel cell based CHP plants installed in different cities in France. In each unit, an electrical power of 5 kW and a low temperature thermal output of 6 kW were obtained. Moreover, Calise et al. [8] analysed an innovative polygeneration system based on solar collectors, absorption chiller and PEM fuel cells which is capable of providing electricity, space heating and cooling, and domestic hot water. Jovan et al. [9] performed an assessment on the actual energetic flows, and consequent electrical efficiency of a case-study PEMFC system. Hubert et al. [10] carried out a steady state modelling and optimization of a small heat and power PEM fuel cell system which is a part of EPACOP project installed in France. In the optimization process while considering constant power output, decreasing the natural gas consumption and increasing the heat recovery were considered as objective functions.

Besides the technical assessments, in any power generation system the economic consideration should also be taken into account [11–14]. In this regard, Contreras et al. [15] carried out an energetic and economic study on a cogeneration system based on PEMFC in rural sector of Venezuela. In another study, Guizzi et al. [16] studied a cogeneration system based on a PEM fuel cell from economic and energetic standpoints. The generated heat in the fuel cell and reformer was utilized to cater the thermal needs of a building. The aforementioned plant has net electric and thermal efficiencies of 41.93% and 64.16% respectively at rated conditions.

High power density, environmentally friendly operation, and solid construction can be known as positive features of the LT-PEM fuel cells. However, there still exist many limitations with these types of fuel cells such as the slow kinetics of oxygen reduction, high material cost of noble catalysts, water management issues, and stack cooling [17,18]. One of the main problems with LT-PEM fuel cell is the poisoning effect of carbon monoxide (CO) in the reformate gas on the platinum anode catalyst which strongly hinders the expected catalyst activity. As a result, a great deal of attention has been paid to alleviate the mentioned disastrous effect of CO in order to boost the performance of the fuel cell [19,20]. One encouraging approach to prevail the shortcoming of the LT-PEM is to increase the PEM fuel cell operating temperature to values higher than 100 °C (high temperature PEM (HT-PEM) fuel cell).

By increasing the temperature, the adverse effect of CO adsorption on the catalyst active sites is diminished. In addition, applying higher temperatures result in easier stack cooling, simpler water management and the possibility of cogeneration applications owing to the high temperature waste heat [21–24].

However, operation at elevated temperatures necessitates some modifications on the membrane material [25,26]. Polybenzimidazole (PBI) has been recognized as one of the most capable choices for high-temperature operation due to its high thermal stability. Furthermore, due to the high operating temperature, water is always in the gas phase and the membrane does not need to be hydrated which simplifies dealing with the flooding and dehydration of mem-brane which are principal problems of conventional LT- PEM fuel cells [1,27,28]. Jannelli et al. [29] carried out an analysis on the per-formance of cogeneration systems based on three different types of fuel cell: an LT-PEM with Nafion™ membrane and two HT-PEM fuel cells with PBI and aromatic polyether polymers as the membranes. Their results demonstrated that the integrated systems based on the HT-PEM fuel cells are characterized by high electrical efficiency of 40% and first law efficiency of 79%. In another study, Arsalis et al.[30] suggested a micro CHP system based on an HT-PEM fuel cell stack with PBI membrane to cater the electric power, domestic hot water and space heating for a typical Danish single family

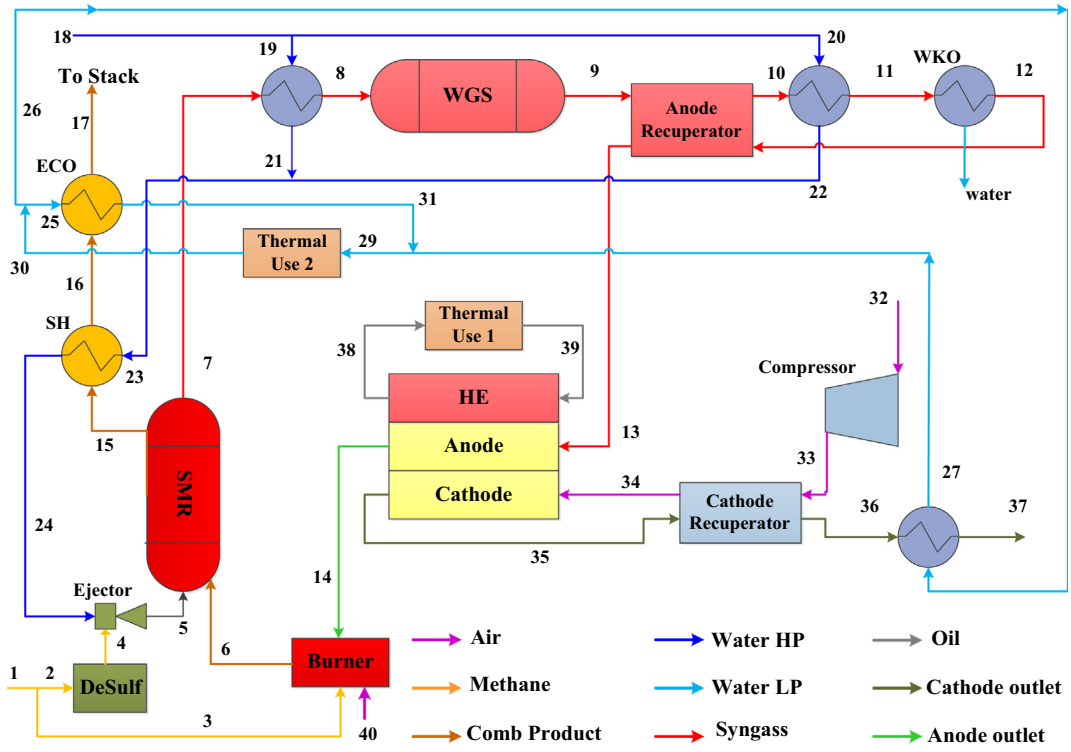

Fig. 1. Configuration of the proposed HT-PEMFC based plant.

household. Zuliani et al. [31] conducted a performance analysis on a 1 kW HT-PEM based cogeneration system fed by natural gas. Their results demonstrated that, at design load, system electrical effi-ciency of 26% and total efficiency of 78% are obtained.

One of the main barriers against the commercialization of PEM fuel cells is the fast degradation of the stack and the subsequent voltage drop in the system. As a result, in recent years, many studies have been undertaken on the recognition of degradation mecha-nisms, prediction of the degradation magnitude, as well as the effective solutions to alleviate the adverse effects [32–35]. In this context, Kim et al. [36,37] proposed a number of experimentally validated models to predict the durability and performance of HT-PEM fuel cell with PBI membrane at different operating tem-peratures. In addition, the study suggested models by incorporating both theoretical and experimental data to find the optimal tem-perature of the stack for a desired lifetime. In another research, Galbiati et al. [38] conducted an experimental study of the degrada-tion of an HT-PEM fuel cell with PBI-based membrane doped with phosphoric acid. It is stated that increasing the temperature from 160 °C to 180 °C resulted in the acceleration of the degradation from 8 $\mu V\,h^{-1}$ to 19 $\mu V\,h^{-1}$. In contrast, they reported that an incre-ment of 0.2 A cm^{-2} (from 0.2 to 0.4 A cm^{-2}) in current density led to a decline in voltage degradation rate to 4 $\mu V\,h^{-1}$, as well as a rise in power output. A similar consideration should also be given to the degradation of fuel processor and specifically reformer reactor; which is mainly contributed to sintering of the catalyst. As a result, it will be inevitable to take into account the impact of reformer degradation on the reformate composition and subsequently the overall long term performance of the cogeneration plant.

In the present study, the long term performance of an HT-PEM fuel cell based micro cogeneration plant fed by natural gas has been studied. From a practical standpoint, the two principal com-ponents of the system, fuel cell stack and steam methane reformer, suffer from a substantial degradation through the lifetime of the system. As a result, in this work the effect of degradation both in the HT-PEM stack and the reformer on the overall performance of the plant has been investigated. Accordingly, the variation in the generated electrical and thermal power and the corresponding efficiencies in the first 15,000 h of operation of the plant have been investigated.

In order to alleviate the deviations of the thermal and electrical power output from the initial level, two strategies have been put forward. In the first strategy, called partialization strategy, through diminishing the fuel supplied to the system, amplification of the thermal generation is suppressed. In this context, in order to evade the deviation of the thermal generation from the initial production, the required fuel reduction at each time interval is determined. Next, the resulting variations in electrical generation of the plant along with the profiles of electrical and thermal efficiencies have been investigated and systematically discussed.

In the recovery strategy, as the second approach, the supplied fuel is gradually increased to inhibit the progressive reduction in the electrical power production. Similarly, the required increment in the provided fuel at each time interval is investigated and main performance indices have been represented.

2. Plant description

The configuration of the proposed CHP system is depicted in Fig. 1. The system is fed by natural gas, which is converted to a hydrogen-rich reformate mixture. To obtain this hydrogen-rich stream, in the first step, the mixture of desulfurized natural gas and superheated steam enters the steam reforming reactor where, via the steam reforming reactions, they are converted into a gaseous mixture of H_2, CO, CO_2 and unreacted H_2O and CH_4.In the second step, in order to achieve an acceptable level of CO content in the syngas entering the stack's anode, the generated SMR outlet stream passes through the WGS reactor in which the shift reaction takes place and a fraction of the CO is converted into CO_2 and additional H_2. The processed syngas afterward enters the anodic side of the HT-PEM fuel cell where the hydrogen is consumed

through the electrochemical reaction generating electricity. The anodic outlet, which still includes unconsumed amounts of hydrogen and methane, is directed to the burner to provide the required energy of the endothermic reactions in SMR reactor and subsequently produce the superheated steam and warm water in the superheater and economizer respectively. If additional air and/or natural gas are needed for the burner, they can be provided by the air blower and the fuel line, respectively. In the other side, the compressed air is fed to the cathodic side providing the required oxygen. In addition, two heat recuperators (anodic and cathodic) are also utilized for warming up the fuel cell inlet streams. It worth noting that the cooling of the fuel cell stack is performed by an oil circulation which is later used by the thermal use 1. Prior to the anodic recuperators, a water knock out (WKO) condenser has been employed to lower the water content of anodic inlet stream. The warm water produced in the heat exchanger placed after the cathodic recuperator is added to the one generated in the economizer and consequently provides thermal energy for the thermal use 2.

Two other heat exchangers, placed before the WGS reactor and after the anodic recuperators, are also employed to lower the temperature of the syngas and for generating high pressure saturated steam which is next introduced into the superheater.

3. Steady state model description

3.1. Fuel processor

3.1.1. Steam methane reformer reactor (SMR)

One of the main technologies for hydrogen production is steam reforming of methane which fulfills more than 50% of the total hydrogen demand worldwide. The kinetic model developed by Xu and Froment [39] for SMR reactor has been employed in the present study. A 1D steady state and non-isothermal plug flow reactor with shell and tube heat exchanger design (in a packed bed arrangement) has been considered for modelling. The model considers two separate working media; the tube side filled with catalysts, in which the reactions take place, and the shell side where the hot gases from the burner pass and cater the required energy for endothermic reforming reactions. The geometry of the modeled SMR reactor is consistent with an experimental setup and the results from the modelling are validated with the real performance of the reactor.

The three main reactions taking place in steam reforming process are as follows:

$$CH_4 + H_2O \Longleftrightarrow CO + 3H_2 \qquad \Delta H_{298K} = +206\ \text{kJ/mol} \tag{1}$$

$$CO + H_2O \Longleftrightarrow CO_2 + H_2 \qquad \Delta H_{298K} = -41\ \text{kJ/mol} \tag{2}$$

$$CH_4 + 2H_2O \Longleftrightarrow CO_2 + 4H_2 \qquad \Delta H_{298K} = +206\ \text{kJ/mol} \tag{3}$$

Due to the fast kinetic of water gas shift reaction, it is accurate enough to consider it in equilibrium. The steam reforming reaction is strongly endothermic and is favoured at low pressure and high temperature. Xu and Froment [39] have developed a general and realistic Langmuir–Hinshelwood type kinetic model for the steam reforming of methane considering the water–gas shift reaction to take place in parallel with the steam reforming reactions. The kinetics equations are:

$$r_I = \frac{k_1}{P_{H_2}^{2.5}} \frac{P_{CH_4}P_{H_2} - P_{H_2}^3 P_{CO}/K_1}{DEN^2} \tag{4}$$

$$r_2 = \frac{k_2}{P_{H_2}} \frac{P_{CO}P_{H_2O} - P_{H_2}P_{CO_2}/K_2}{DEN^2} \tag{5}$$

$$r_3 = \frac{k_3}{P_{H_2}^{3.5}} \frac{P_{CH_4}P_{H_2O}^2 - P_{H_2}^4 P_{CO_2}/K_3}{DEN^2} \tag{6}$$

$$DEN = 1 + K_{CO}P_{CO} + K_{H_2}P_{H_2} + K_{CH_4}P_{CH_4} + \frac{K_{H_2O}P_{H_2O}}{P_{H_2}} \tag{7}$$

$$k_i = A(k_i)\cdot \exp[-E_i/(RT)], \quad \text{for } i = 1, \ldots, 3 \tag{8}$$

$$K_i = A(K_i)\cdot \exp[-\Delta H_i/(RT)], \quad \text{for } i = 1, \ldots, 3 \tag{9}$$

$$K_j = A(K_j)\cdot \exp[-\Delta H_j/(RT)], \quad \text{for } j = CH_4, H_2O, CO, H_2 \tag{10}$$

3.1.2. Water gas shift reactor

Aiming to supply high yield of hydrogen and also remove the carbon monoxide which is harmful to the stack, the water gas shift (WGS) reaction is carried out on the SMR outlet syngas:

$$CO + H_2O \Longleftrightarrow CO_2 + H_2 \qquad \Delta H_{298K} = -41\ \text{kJ/mol} \tag{11}$$

The heat exchanger placed before the WGS reactor decreases the temperature of the inlet stream to WGS reactor to a favourite level. In addition, although the experimental data suggest that the addition of water in the WGS reactor can increase the carbon monoxide conversion, here no additional source of water has been introduced for WGS reaction. The principal reason is that higher amount of water may burden extra load to the water knockout stage which adjusts the amount of water in the anode inlet. The thermodynamic equilibrium constant of the WGS reaction can be expressed as:

$$K_p = e^{\left(\frac{4400}{T} - 4.036\right)} \tag{12}$$

For the shift converter, the kinetics equation according to Keiksi et al. [40] for high temperature WGS is:

$$r_{WGS} = k_0 \cdot \exp\left(\frac{-E_a}{RT}\right)(1-\beta)P_{CO}^{1.1}P_{H_2O}^{0.53} \tag{13}$$

where E_a = 95,000 kJ/mol is the activation energy, R = 8.314 J/(K mol), ln (k_0) = 26.1 is pre-exponential factor, and β is the reversibility factor defined as:

$$\beta = \frac{1}{K_P}\frac{P_{CO_2}P_{H_2}}{P_{CO}P_{H_2O}} \tag{14}$$

3.2. HT-PEMFC stack

The HT-PEM fuel cell stack consists of three parts including the pre-heater, the oil cooling circuit and the membrane electrode assembly (MEA). In the preheater section, the compressed air and the syngas entering the stack, by exchanging heat with the cooling oil, reach the desirable range of temperature for the stack. On the other hand, the electrochemical reaction, through which the supplied hydrogen and oxygen are consumed while generating electrical power and producing water, takes place in MEA zone. Three main parts can be recognized in the MEA domain which are the cathode (and anode) channels where the air (and syngas) inlet flow passes through, the cathode (and anode) gas diffusion layer (GDL) a pathway for reactants to reach catalyst layer, and the cathode and anode electrodes where the electrochemical conversion happens. In the ideal case, the electrolyte, which separates the electrodes, should only allow the flow of protons. Two hypotheses have been considered while developing the fuel cell model: (1) pressure drop along the channels is negligible; (2) the reactants divide equally in

Table 1
The geometric parameters of the HT-PEM fuel cell based stack.

Geometric parameter	Value
Channel length (cm)	76.25
Channel height (cm)	0.2
Cell width (cm)	7.6
Number of channels	38
Number of cells	440

Table 2
The values of the parameters used for the HT-PEM fuel cell modelling.

Symbol	Value	Description
C_{ref} (mol cm^{-3})	$5.88 \cdot 10^{-6}$	Reference O_2 concentration
δ_{GDL} (cm)	0.04	GDL thickness, anode/cathode
δ_{MEM} (cm)	0.015	Membrane thickness [45]
ε/τ_{GDL} (–)	0.084	Porosity/tortuosity GDL, anode/cathode
$\theta_{H_2PO}^{4-}$ (–)	0.05	$H_2PO_4^-$ coverage [45]
E_0 (V)	1.256–$2.4 \cdot 10^{-4}$ T	Ideal potential
α_C (–)	0.85	Charge transfer coefficient cathode [41]
E_{ORR} (J mol^{-1})	$102.86 \cdot 10^3$	Activation energy ORR [45]
$i_{0,ORR}$ (A cm^{-2})	$3.28 \cdot 10^{-6}$	Exchange current density ORR [45]
α_A (–)	0.5	Charge transfer coefficient anode [45]
E_{HOR} (J mol^{-1})	$2.5 \cdot 10^3$	Activation energy HOR
$i_{0,HOR}$ (A cm^{-2})	$1.25 \cdot 10^3$	Exchange current density HOR [20]
$E_{COR,C}$ (J mol^{-1})	$127 \cdot 10^3$	Activation energy COR [20]
$i_{0,COR}$ (A cm^{-2})	$2.2 \cdot 10^{13}$	Exchange current density cathode [20]
$E_{ADS,H}$ (J mol^{-1})	$10.4 \cdot 10^3$	Activation energy hydrogen adsorption [20]
$k_{ADS,H}$ (cm s^{-1})	5.96	Hydrogen adsorption constant [20]
$E_{ADS,CO}$ (J mol^{-1})	$47.3 \cdot 10^3$	Activation energy CO adsorption [20]
$k_{ADS,CO}$ (cm s^{-1})	$1.5 \cdot 10^5$	CO adsorption constant [45] Activation
$E_{DES,H}$ (J mol^{-1})	$98.3 \cdot 10^3$	energy hydrogen desorption [20] Hydrogen desorption constant [20]
$k_{DES,H}$ (cm s^{-1})	$2.5 \cdot 10^3$	Activation energy CO desorption [20]
$E_{DES,CO}$ (J mol^{-1})	$147 \cdot 10^3$	CO desorption constant [20]
$k_{DES,CO}$ (cm s^{-1})	$1.03 \cdot 103$	Frumkin isotherm symmetry factor [20]
β_{CO} (–)	0.1	Frumkin isotherm lateral interaction
r_{CO} (J mol^{-1} K^{-1})	56.5	parameter [20] GDL conductivity [44]
σ_{GDL} (S cm^{-1})	9	Membrane conductivity parameter [41]
σ_0 (S cm^{-1} K^{-1})	$9.4 \cdot 10^3$	Activation energy membrane
$E_{\sigma,MEM}$ (J mol^{-1})	$18.5 \cdot 10^3$	conductivity [41] Membrane water permeation coefficient
D_m (cm^2 s^{-1})	0.001	

each channel, which gives the possibility to simulate a single channel and extend the results to the whole stack.

The MEA domain is simulated with the quasi 2D approach: the channel is monodimensional in the flow direction and monodimensional through the MEA direction. The mass conservation is applied in order to calculate the species concentration profiles along the channels, especially oxygen, hydrogen, water and carbon monoxide. The design data of the stack are reported in Table 1.

The reaction rate (the current density) is computed locally by solving the following identity which relates the cell voltage to the ideal voltage:

$$V = E_{ID} - \eta_{OHM} - \eta_C - \eta_A \quad (15)$$

$$P_{stack} = V_{cell} I_{stack} N \quad (16)$$

where V is the single cell voltage, E_{ID} is the ideal voltage, η_{OHM} is the Ohmic loss, and η_C and η_A are the cathode and anode activation losses respectively. The ideal voltage (E_{ID}) is computed as a function of temperature from the Gibbs free energy formation data and the Ohmic loss is the sum of bipolar plate, GDLs and electrolyte resistances. The electrolyte conductivity follows Arrhenius law and it is taken from [41]. Mass transport in the GDL is simulated considering multi component gas diffusion by means of Stefan-Maxwell phenomenological law [42]. The binary diffusion coefficients are computed by means of the correlation by Fuller et al.[43] and later corrected to account for the porous media porosity and tortuosity.

The cathode electrode is considered as homogeneous and activation losses are supposed to follow the Tafel Law, first order with respect to oxygen concentration [44]:

$$\eta_C \equiv b \cdot \log\left(\frac{i}{i_*}\right) + b \cdot \log\left(\frac{C_{ref}}{C_{O2,el}}\right) \quad (17)$$

where i_* is the reference exchange current density which follows an Arrhenius like behaviour and

$$b = RT/(\alpha_C F) \quad (18)$$

is the Tafel slope.

As it was stated before, CO has poisoning effect on the catalyst of the anodic side. As a result, the impact of this CO adsorption on the catalyst active sites on voltage has been considered in the activation loss at the anode. The hydrogen and CO oxidation currents are computed by means of the Butler–Volmer equation [20]:

$$i_{H2} \equiv i_{*,H2} \cdot \vartheta_H \cdot 2\sinh\left(\frac{\eta_A}{b_A}\right) \quad (19)$$

$$i_{CO} \equiv i_{*,CO} \cdot \vartheta_{CO} \cdot 2\sinh\left(\frac{\eta_A}{b_A}\right) \quad (20)$$

$$i = i_{CO} + i_{H2} \quad (21)$$

where the coverage of all the species must sum to 1 by definition:

$$\vartheta_{FREE} = 1 - \vartheta_H - \vartheta_{CO} - \vartheta_{H_2PO_4^-} \quad (22)$$

The coverage of phosphoric acid (ϑ_{H2PO4-}) is taken from [45], and in case of hydrogen and CO coverage (ϑ_H and ϑ_{CO}) are computed considering the equilibrium of adsorption using Frumkin adsorption for CO and Langmuir adsorption for hydrogen.

In HT-PEM, the presence of phosphoric acid facilitates the proton transport through the membrane even in high conditions of dehydration (RH < 5%). The main mechanism is of Grotthus type. Due to the amphoteric characteristics of phosphoric acid, a chain can be formed which helps the protons to pass through the membrane. The transport of water through the membrane has a diffusive character and can be represented by Fick's law, assuming equilibrium of water in the vapour phase and in acid at the interface of the electrode.

The values of the parameters used for the HT-PEM fuel cell stack modelling in the present study are summarized in Table 2.

3.3. Auxiliary components

3.3.1. Ejector

As was previously explained the high temperature steam which has been produced in the superheater and the process methane in the first step enter the ejector. For simulating the behaviour of the ejector, the single phase thermodynamic model presented in [46], based on isobaric mixing, has been utilized in which the ejector structure is divided into four main sections of the nozzle, the suction chamber, the constant and the diffuser.

3.3.2. Heat exchangers

In order to model the heat exchangers, an iterative LMTD method has been employed. In order to calculate the global heat transfer coefficient, the internal and external convective heat transfer coefficients should be evaluated. The Churchill–Bernstein relation for cross flow heat exchange over tubes is used for determining the external convective heat transfer coefficient [47,48]

$$Nu_D = 0.3 + \frac{0.62 Re_D^{1/2} Pr^{1/3}}{\left[1 + \left(\frac{0.4}{Pr}\right)^{2/3}\right]^{1/4}} \left[1 + \left(\frac{Re_D}{282{,}000}\right)^{5/8}\right]^{4/5} \quad (23)$$

Table 3a
Outlet dry molar fractions of the SMR and WGS reactors obtained from the model and the provided experimental data.

Dry molar fraction	CH_4	H_2	CO	CO_2	N_2
SMR outlet (experimental)	0.0452	0.749	0.051	0.151	0.0047
SMR outlet (model)	0.0528	0.745	0.0478	0.1504	0.00418
WGS outlet (experimental)	0.045	0.753	0.012	0.1856	0.0044
WGS outlet (model)	0.0508	0.754	0.00865	0.182	0.00403

Table 3b
Outlet temperatures of the fuel processor reactors and superheater obtained from the model and the provided experimental data.

Parameter	Model (°C)	Experimental (°C)
Syngas temperature at SMR outlet	577	590
Syngas temperature at WGS outlet	339	331
Steam temperature at superheater outlet	535	527

For calculation of the internal heat transfer coefficient, Gnielinski equation is utilized [47]:

$$Nu_D = \frac{(f/8)(Re_D - 1000)Pr}{1 + 12.7(f/8)^{1/2}(Pr^{2/3} - 1)} \quad (24)$$

4. Model validation

The kinetic characteristics and geometric parameters of the steam methane reformer and the water gas shift reactors (employed in the present HT-PEM based plant) are taken from an LT-PEM fuel cell based CHP plant (Sidera30), designed by ICI Caldaie S.p.A, a prototype of which was previously installed in Department of Energy of Politecnico di Milano. Accordingly, the validation of the fuel processor model is carried out utilizing the experimental data of the fuel processor of the LT-PEM based system. Therefore, while working at operating conditions of the LT-PEM based system, the syngas composition at the outlet of the reformer and WGS reactors obtained by the model are compared with the corresponding experimental data. The temperature of the syngas leaving the fuel processor reactors and the superheater outlet temperature are also compared with the corresponding values extracted from the experimental data. As presented in Table 3, despite the subtle difference between the values obtained by the model and the experimental data, it can be observed that the models can predict the performance of the fuel processor with a good agreement with the experimental data.

In order to validate the HT-PEM fuel cell model, the polarization curves of the fuel cell obtained from the developed model and the experimental data given by Bergmann et al. [45] at different temperatures (130–160 °C) and with pure hydrogen and CO concentration of 1.6% have been compared. The conducted comparison, demonstrated in Fig. 2 verifies the sufficient accuracy of the developed model for simulating the behaviour of the HT-PEM fuel cell.

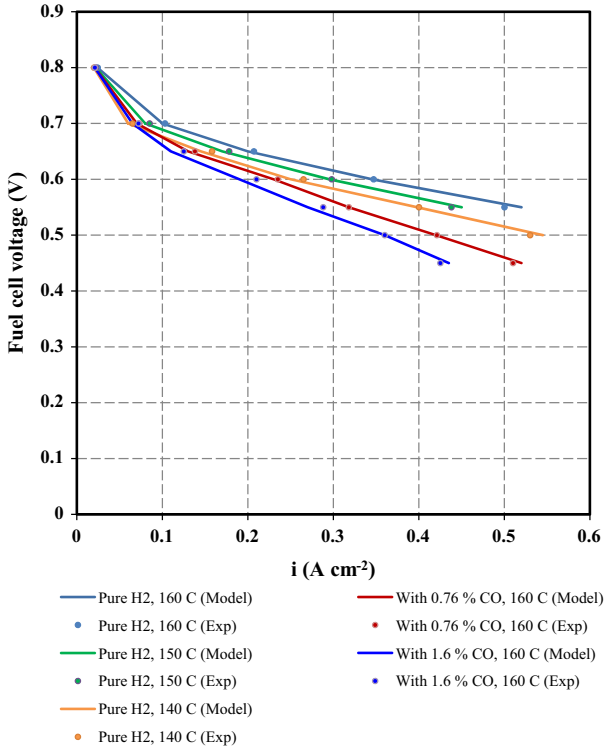

Fig. 2. Validation of the developed model for the HT-PEM fuel cell stack.

5. Degradation models

5.1. Reformer degradation

In order to estimate the degradation within the steam reformer, the experimental data of the long term performance of the steam reformer, provided by the ICI Caldaie S.p.A and derived from the fuel processor of an operating LT-PEM fuel cell based micro CHP system (Sidera30), has been employed via an empirical correlation. The provided experimental data is tabulated in Table 4.

5.2. HT-PEM stack degradation

Co-authors of the present work conducted an experimental study on the degradation of a PBI-based HT-PEM fuel cell and investigated the effect of the operating temperature, current density and the cathodic stoichiometry on the degradation rate [38]. Accordingly, as the first analysis they analysed a cell, operat-ing at anodic stoichiometry of 1.2, cathodic stoichiometry of 2 and cell temperature of 160 ° C, and determined the corresponding degradation rate of the cell in the first 1000 h to be 8 $\mu V\,h^{-1}$. In another comprehensive study, Kim et al. [36] proposed a number of experimentally validated models to predict the durability and performance of HT-PEM fuel cell stack for longer operation periods and different cell temperatures. The obtained results from the experimental correlation suggested by Kim et al. [36] is consistent with the experimental value obtained by the co-authors [38]. Considering the fact that the fuel cell employed in the present plant is of similar characteristics as the one studied by Kim et al.[36], and assuming that the degradation is mainly occurring in the cathodic side and the membrane of the cell, the model proposed by Kim et al. [36] has been utilized in the present study to predict the degradation within the HT-PEM stack. Fig. 3 demonstrates the profile of cell voltage drop due to the degradation as estimated by the employed model.

6. Results and discussions

6.1. Steady state performance

As the first analysis of the present study, the steady state performance of the plant in the beginning of the operation (time = 0) is studied. The operating conditions which have been applied for the analysis are given in Table 5.

Considering the interconnection between the components of the plant, an iterative procedure has been employed in order to obtain the converged results of the performance of the system. In this context, guess values are first considered for the composition at the anodic outlet stream and the water temperature at the superheater outlet. Employing the developed component models, the stream composition and the temperatures at different nodes of the plant are calculated accordingly and the determined values of anodic outlet stream's composition and the superheater's outlet water temperature are compared with the guess values. The guess values are accordingly modified, in an iterative loop, until the

Table 4
Reformer performance in different operating time.

Time	0	2000	4000	6000	8000	10,000	12,000	14,000
Conversion (%)	75.2	72.9	71.3	70.6	69.9	69.4	69.2	69

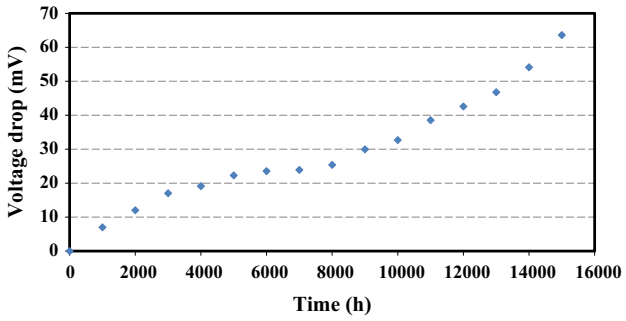

Fig. 3. Voltage drop due to the degradation in time.

differences between the guessed and determined value are less than the assumed tolerance. The resulting performance indexes of the system have been shown in Table 6. As can be observed, the electrical power of 28.23 kW is produced while 52.35 kW of total thermal power can also be gained from the system. Accordingly, electrical and thermal efficiencies of 28.95% and 53.70% are achieved respectively at the starting moment of opera-tion. Ultimately, in order to evaluate the advantage of the cogenerative plant with respect to conventional separate power and thermal generation systems, primary energy savings (PES) index of the plant is also calculated and is determined to be 17.12% which affirms high efficiency of the cogenerative system. It is worth mentioning that based on the Italian implementation of the EU directive on cogeneration, for calculating the primary energy savings (PES) index, the reference electrical and thermal efficiencies for the separate generation of electricity and heat are considered to be 52.5% and 90% respectively. It is also assumed that 50% of electricity production of the plant is consumed onsite and 50% is injected to the local grid, therefore the intermediate grid efficiency coefficient, is equal to 0.8925 [49].

6.2. Long-term performance investigation

With the aim of investigating the effect of the degradation in the steam reforming reactor and the stack on the system, the performance of the plant in the first 15,000 h of operation has been studied. Fig. 4 displays the variation in the electrical and thermal generations of the plant. A steady decrement in the generated electrical power of the plant, from 28.2 kW (in the beginning of operation) to 23.4 kW after 15,000 h, evidences the noticeable effect of degradation on the performance of the system. Evidently, the significant decrement in the electrical efficiency in the first few thousand hours of operation, is a consequence of the sharp drop in the methane conversion due to the reformer degradation. On the other hand, the major decrease at the end of the investigated period can be attributed to the harsh rise in the degradation of the stack, the fact which can also be observed in the variations of the cell voltage given in Fig. 5 and the estimated voltage drops demonstrated in Fig. 3.

The generated thermal power of the system, which is 52.3 kW at the beginning of operation, experiences a gradual increase reaching 57.5 kW at the end of the studied period. The evidenced growth in thermal generation through the time could be foreseen due to two major reasons. Firstly, voltage losses' increase stemming from the stack degradation leads to an increment in the waste heat of the stack and consequently the thermal output. On the other hand, the reformer aging imposes a remarkable catalyst degradation which brings about lower rate of endothermic steam reforming reactions. Consequently, lower heat is absorbed in the reforming reactor resulting in higher outlet temperature of the combustion products; the fact which eventuates in an increment in the economizer thermal gain and the overall thermal output.

In view of the mentioned thermal and electrical generation profiles, the electrical efficiency is steadily reduced from 28.95% to 23.97% while the thermal efficiency keeps its ascending trend from the initial value of 53.7% to 59.0% after 15,000 h.

6.3. Operational strategies

In the following sections, two operational strategies, based on changing the mass flow rate of the fuel fed to the system, have been proposed in order to mitigate the variations in the electrical and thermal production of the plant due to the degradation within the system. It is worth mentioning that employing the physical model, which has been developed in the present study based on the correlations which are valid in a wide range of operating conditions, has provided the possibility to simulate the behaviour of the system in off design conditions with an acceptable accuracy. Furthermore, it is also assumed that a thermal storage tank is utilized and the system is designed to operate only in the winter season (the period in which the building's thermal demand is more than the plant's thermal production). Nonetheless, it should be pointed out that, in case the system is designed to supply the whole demand of the building, the nature of thermal and electrical profiles will be a key factor in determining the performance indices of the plant.

6.3.1. Partialization strategy

As the first strategy in the present study, the thermal production of the system is considered to be kept constant. In fact, the plant is designed to meet a specific portion of the building's thermal demand. As demonstrated in the previous section, the thermal

Table 5
Operating parameters of the system.

Operating condition	Value
Steam to carbon ratio (S/C)	4.5
Auxiliary to process flow rate ratio	0.14
Anodic stoichiometric ratio	1.2
Cathodic stoichiometric ratio	2
Current density (A cm^{-2})	0.2
Combustor outlet temperature (°C)	920
Cell temperature (°C)	160

Table 6
Performance indexes of the CHP plant at the beginning of operation.

Performance index	Value
Generated net electrical power (kW)	28.23
Generated total thermal power (kW)	52.35
Electrical efficiency (%)	28.95
Thermal efficiency (%)	53.70
First law efficiency (%)	82.66
PES (%)	17.66

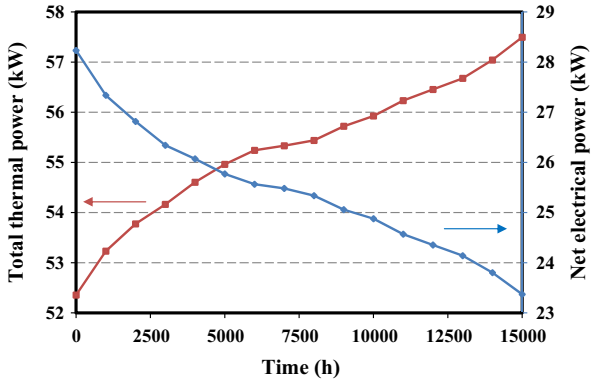

Fig. 4. Variations of the generated electrical and thermal power of the plant in normal operation.

generation of the plant, due to degradation, is continuously increasing. As a result, in order to keep the thermal generation in a narrow range, a partialization strategy has been utilized. Hence, at each specific time interval, an iterative procedure is carried out to find the required decrement in the amount of the process fuel fed to the plant. The iterative procedure is conducted at each 1000 h and the corresponding required reductions in the fuel are determined. In order to have a proper index, the partialization factor is defined as the ratio of the amount of decrease in the fuel fed and the plant's initial fuel consumption. It is noteworthy that through the partialization procedure, the imposed current of the stack is gradually decreased in order to keep the utilization factor constant and equal to its initial value. The obtained results, shown in Fig. 6, demonstrate that in order to keep the deviation of thermal generation in a narrow range, the partialization factor should be gradually increased up to 7.2%.

As can be observed in Fig. 7, the electrical output will be accordingly decreased down to 22.16 kW at the end of studied period which shows a lower power generation compared to the one obtained for the system operating in normal condition (23.37 kW). Nevertheless, it should be noted that the electrical efficiency, as demonstrated in Fig. 8, goes down to 24.50% at the end of investigated period which is slightly higher than the value obtained in the long term analysis (23.97%). Accordingly, the partialization approach, aside from keeping thermal output at a reasonable level, can also slightly mitigate the destructive effect of degradation on the electrical efficiency. The mentioned alleviating effect of partialization strategy is attributed to two different effects of this strategy. Firstly, as the amount of fuel fed to the plant is decreasing, the current of the stack should be gradually reduced while the area of the stack is constant, hence the current density is diminished and higher cell voltage, in comparison with the normal operation of the plant, is obtained. Secondly, decreasing the process fuel, in the specific operating condition of the plant, leads to a higher hydrogen yield. Although the thermal generation of the plant has been confined in a narrow range, the supplied fuel is gradually reduced; therefore, as depicted in Fig. 8, the thermal efficiency experiences an ascending trend reaching to 58.02%.

6.3.2. Recovery strategy

In some cases, the micro-CHP system is just providing a part of the thermal demand and the major required thermal load is met by the conventional boiler. In such cases it might be desired for the owner to keep the power production of the unit within a confined range and subsequently maintain the profit gained from selling the generated electricity to the grid. Therefore, as the second approach, a recovery strategy is implemented in which the gradual decrement in the power generation of the system is compensated by increasing the fuel fed to the system. Accordingly, in order to restrict the deviation of the power production, the required increase in the supplied fuel in each time interval has been determined. Based on the achieved results, shown in Fig. 9, the recovery factor which is the percentage of increment in the provided fuel compared to the initial value should be gradually increased up to 0.34 at the end of operation. The electrical efficiency undergoes a sharp fall and, as represented in Fig. 8, is reduced to 21.57% at the end of investigated period. The achieved electrical efficiency at the end of the operation is lower than the corresponding value, obtained by normal operation, owing to two different effects. First, increasing the fuel fed, despite increasing the total flow rate of the produced hydrogen, reduces the methane to hydrogen conversion. Secondly, the augmented hydrogen flow rate fed to the stack eventuates in higher current density which in turn amplifies the voltage losses and lowers the stack production and consequently the overall electrical efficiency of the plant. In this context, the thermal generation of the plant is also substantially augmented as the total flow rate of the fuel fed to the plant is enhanced while both the steam reformer and the fuel cell stack are becoming less efficient. The heat waste and the consequent thermal generation of the stack and also the heat gain of the economizer downstream of the reformer will be noticeably boosted leading to a remarkable growth in the overall power generation.

6.4. Comparison of performance of the system under applied operating strategies

Although each of the mentioned operational strategies can be applied in different cases, comparing the efficiency of the system and the overall generated electrical energy can give insightful

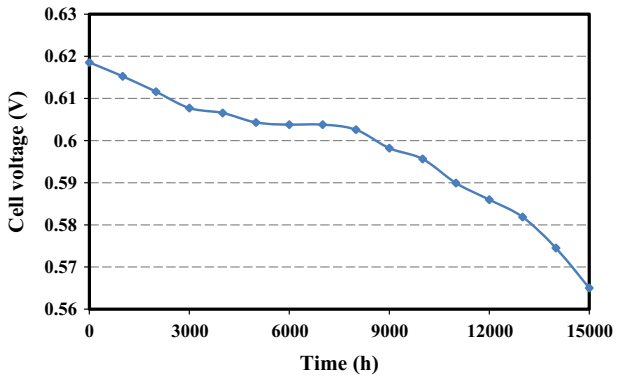

Fig. 5. Variations of the cell voltage in the normal operation.

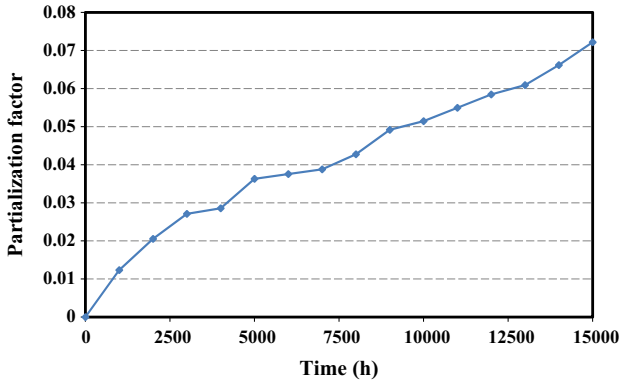

Fig. 6. Variation of the determined partialization factor.

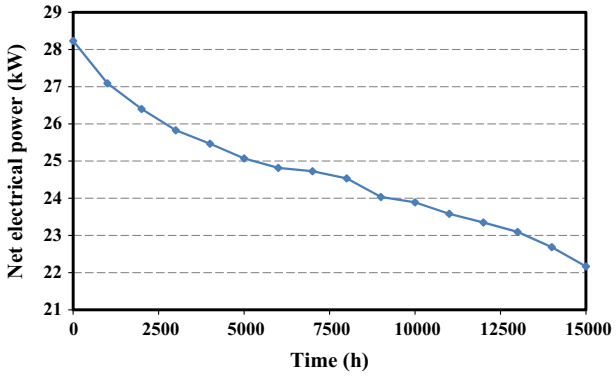

Fig. 7. The profile of generated net electrical power obtained using partialization strategy.

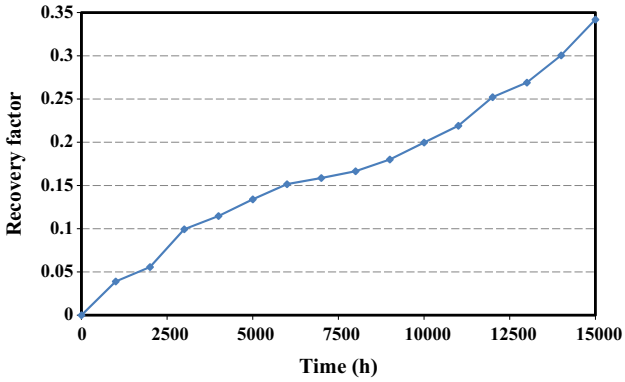

Fig. 9. Variations of the obtained recovery factor for the recovery strategy.

indications for choosing an appropriate strategy. Accordingly, the variations in the cell voltage of the stack, while operating in normal conditions and under partialization and recovery strategies, are demonstrated in Fig. 10. As can be noticed, operating under partialization strategy can have a mitigating effect on the decrement in the cell voltage, the recovery strategy can have a considerable negative effect resulting a considerably lower voltage. The observed beha-viour, as was also previously discussed, corresponds to the fact that increasing the provided fuel, in the recovery strategy, leads to an increment in the current density and consequently a drop in the cell voltage. Besides, feeding the reformer with more fuel leads to a decrease in the methane to hydrogen conversion. The mitigat-ing effect of partialization strategy can also be attributed to the same phenomenon as decreasing the fuel results in a decrement in the current density and increase in the methane conversion. A similar behaviour can also be noted in Fig. 11, which demonstrates the variations in the cumulative electrical efficiency. The cumulative electrical efficiency at each time step is determined by dividing the total energy produced since the beginning of operation till the end of that time step, to the total energy consumed in the whole period. As can be observed in Fig. 11, normal operation, for 15,000 h, results in a cumulative electrical efficiency of 26.1%,

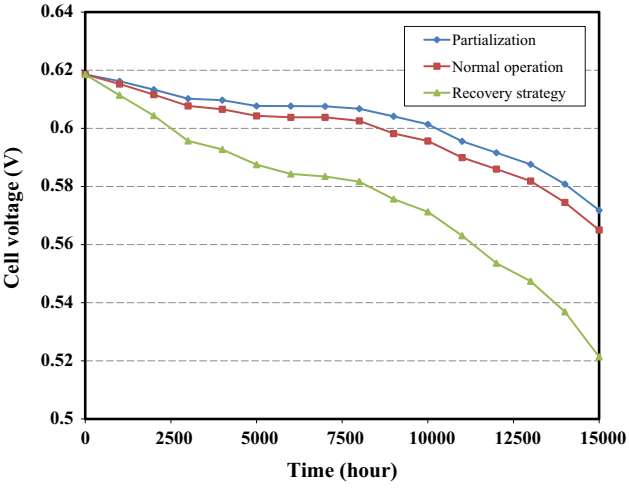

Fig. 10. Variations of the cell voltage gained in normal operation and using different strategies.

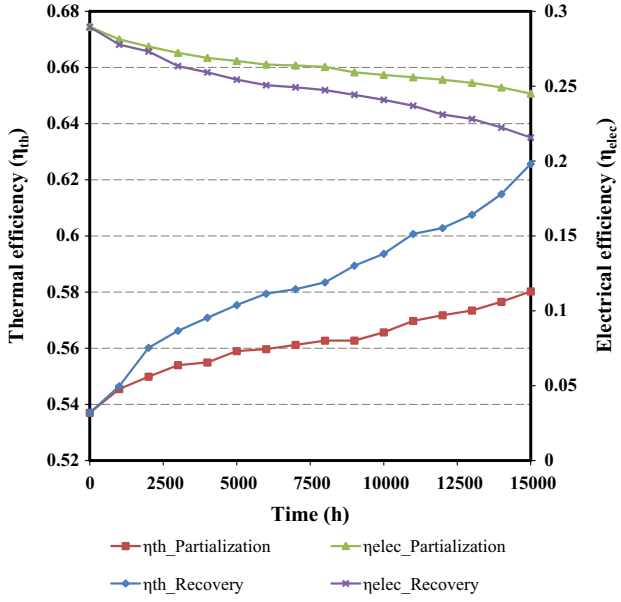

Fig. 8. Variations of electrical and thermal efficiency obtained using partialization and recovery strategy.

while operating under partialization strategy increases the gained value to 26.4% and applying the recovery strategy can reduce the obtained cumulative electrical efficiency to 24.7%. Hence, the designer should keep in mind the significant reduction in the overall electrical efficiency of the plant while applying the recovery strategy. Another index which should be taken into account, while analysing the operational strategies, is the total electrical energy produced by the plant during the investigated period. Fig. 12 demonstrates the cumulative electrical energy generated by the plant while operating in normal condition and under operational strategies. As can be observed in this diagram, while by operating in normal condition or applying the partialization strategy, 381.3 MW h and 369.8 MW h of electrical energy can respectively be generated by the system in 15,000 h, operation under recovery strategy results in production of 422.6 MW h of electrical energy. Hence, despite resulting in lower overall performance, operating under recovery strategy results in higher overall production; the fact which should be considered while analysing the applied operational strategies from the economical point of view.

7. Conclusions

As the first analysis, the variations in the performance indexes of an HT-PEM fuel cell based micro CHP plant, in the first 15,000 h of operation, due to the degradation of the stack and

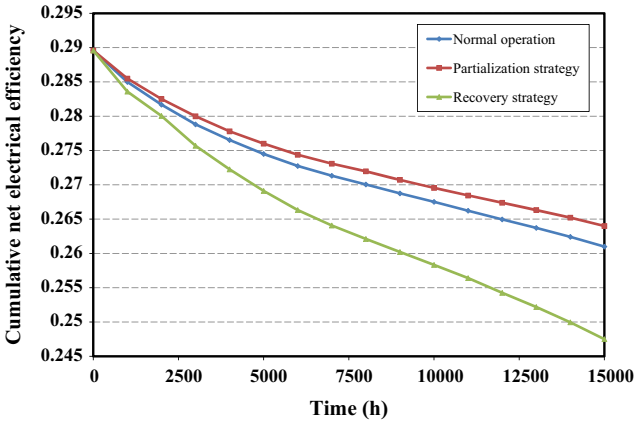

Fig. 11. Variations in the cumulative electrical efficiency in normal operation and under operational strategies.

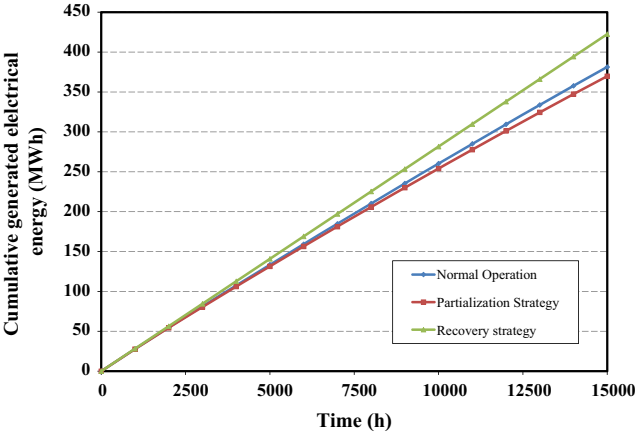

Fig. 12. Variations in the cumulative generated power in normal operation and under operational strategies.

the steam reformer reactor was investigated. Accordingly, the variations in the generated electrical and thermal power and the corresponding efficiencies in the first 15,000 h of operation of the plant have been investigated. The physical model developed in this study, based on the correlations which are valid in a wide range of operating conditions, is a valid instrument for analysing the operational strategies for stabilizing the output of the cogeneration system based on the desired application. Accordingly, two strategies have been proposed and applied in order to remedy the excursion of thermal and electrical generation of the plant from the steady state production. In the partialization strategy, by means of reducing the fuel fed to the system, the thermal generation of the plant is kept in a specified range. On the other hand, in the recovery strategy, the supplied fuel is gradually increased to suppress the progressive reduction in the power production.

The long term performance analysis, in normal conditions, reveals that, due to the degradation within the system, the power production diminishes from 28.2 kW to 23.4 kW while the thermal generation increases from 52.4 kW to 57.5 kW. The results of partialization strategy show that, in order to confine the thermal generation amplification, the partialization factor should be increased up to 7.2%. On the other hand, in the recovery strategy, the supplied fuel should be progressively increased up to 34.2% in order to preserve the electrical output at the initial level. Nevertheless, the recovery strategy has an adverse effect on the electrical efficiency as it diminishes the obtained to 21.6% compared to 24% obtained in normal operation. In the last step, the performance of the system obtained by normal operation and under proposed operational strategy was compared. It was shown that applying the recovery strategy can result in an overall electrical efficiency of 24.7%, through the investigated period, which is considerably lower than the efficiencies obtained by operating in normal condition and under partialization strategy which are 26.1% and 26.4% respectively. Nevertheless, it was also demonstrated that applying the recovery strategy results in the generation of 422.6 MW h of electrical energy which is notably higher than 381.3 MW h and 369.8 MW h of energy which are generated while operating in normal condition and partialization strategy; The fact which should be taken into account while analysing the operational strategies from economical point of view.

Acknowledgment

The authors would like to acknowledge ICI Caldaie S.p.A for providing technical and financial support for this project.

References

[1] Mancusi E, Fontana É, Ulson de Souza AA, Guelli Ulson de Souza SMA. Numerical study of two-phase flow patterns in the gas channel of PEM fuel cells with tapered flow field design. Int J Hydrogen Energy 2014;39:2261–73.
[2] Liu H, Li P, Wang K. Optimization of PEM fuel cell flow channel dimensions – mathematic modeling analysis and experimental verification. Int J Hydrogen Energy 2013;38:9835–46.
[3] Rinaldi F, Marchesi R. Polimeric electrolyte membrane fuel cells: characterization test under variable temperature and relative humidity conditions. J Fuel Cell Sci Technol 2006;4:231–7.
[4] Najafi B, Haghighat Mamaghani A, Baricci A, Rinaldi F, Casalegno A. Mathematical modelling and parametric study on a 30 kWel high temperature PEM fuel cell based residential micro cogeneration plant. Int J Hydrogen Energy 2015;40:1569–83.
[5] Ferguson A, Ismet Ugursal V. Fuel cell modelling for building cogeneration applications. J Power Source 2004;137:30–42.
[6] Radulescu M, Lottin O, Feidt M, Lombard C, Le Noc D, Le Doze S. Experimental and theoretical analysis of the operation of a natural gas cogeneration system using a polymer exchange membrane fuel cell. Chem Eng Sci 2006;61:743–52.
[7] Ersöz A. Investigation of hydrocarbon reforming processes for micro-cogeneration systems. Int J Hydrogen Energy 2008;33:7084–94.
[8] Calise F, Ferruzzi G, Vanoli L. Transient simulation of polygeneration systems based on PEM fuel cells and solar heating and cooling technologies. Energy 2012;41:18–30.
[9] Jovan V, Perne M, Petrovčič J. An assessment of the energetic flows in a commercial PEM fuel-cell system. Energy Convers Manag 2010;51:2467–72.
[10] Hubert C-E, Achard P, Metkemeijer R. Study of a small heat and power PEM fuel cell system generator. J Power Sources 2006;156:64–70.
[11] Mamaghani AH, Najafi B, Shirazi A, Rinaldi F. Exergetic, economic, and environmental evaluations and multi-objective optimization of a combined molten carbonate fuel cell-gas turbine system. Appl Therm Eng 2015;77:1–11.
[12] Haghighat Mamaghani A, Najafi B, Shirazi A, Rinaldi F. 4E analysis and multi-objective optimization of an integrated MCFC (molten carbonate fuel cell) and ORC (organic Rankine cycle) system. Energy.
[13] Aminyavari M, Najafi B, Shirazi A, Rinaldi F. Exergetic, economic and environmental (3E) analyses, and multi-objective optimization of a CO_2/NH_3 cascade refrigeration system. Appl Therm Eng 2014;65:42–50.
[14] Shirazi A, Najafi B, Aminyavari M, Rinaldi F, Taylor RA. Thermal-economic-environmental analysis and multi-objective optimization of an ice thermal energy storage system for gas turbine cycle inlet air cooling. Energy 2014;69:212–26.
[15] Contreras A, Posso F, Guervos E. Modelling and simulation of the utilization of a PEM fuel cell in the rural sector of Venezuela. Appl Energy 2010;87:1376–85.
[16] Guizzi GL, Manno M. Fuel cell-based cogeneration system covering data centers' energy needs. Energy 2012;41:56–64.
[17] Cheddie D, Munroe N. Mathematical model of a PEMFC using a PBI membrane. Energy Convers Manag 2006;47:1490–504.
[18] Li Q, He R, Jensen JO, Bjerrum NJ. PBI-based polymer membranes for high temperature fuel cells – preparation, characterization and fuel cell demonstration. Fuel Cell 2004;4:147–59.
[19] Baschuk JJ, Li X. Carbon monoxide poisoning of proton exchange membrane fuel cells. Int J Energy Res 2001;25:695–713.
[20] Baschuk JJ, Li X. Modelling CO poisoning and O_2 bleeding in a PEM fuel cell anode. Int J Energy Res 2003;27:1095–116.
[21] Zhang J, Xie Z, Zhang J, Tang Y, Song C, Navessin T, et al. High temperature PEM fuel cells. J Power Source 2006;160:872–91.

[22] Gao X, Andreasen SJ, Chen M, Kær SK. Numerical model of a thermoelectric generator with compact plate-fin heat exchanger for high temperature PEM fuel cell exhaust heat recovery. Int J Hydrogen Energy 2012;37:8490–8.
[23] Andreasen SJ, Vang JR, Kær SK. High temperature PEM fuel cell performance characterisation with CO and CO_2 using electrochemical impedance spectroscopy. Int J Hydrogen Energy 2011;36:9815–30.
[24] Rossi F, Nicolini A, Di Profio P. Small size cylindrical molten carbonate fuel cells and future approaches for decreasing working temperature. ECS Trans 2008; 1st ed.:455–66.
[25] Korsgaard AR, Refshauge R, Nielsen MP, Bang M, Kær SK. Experimental characterization and modeling of commercial polybenzimidazole-based MEA performance. J Power Source 2006;162:239–45.
[26] Oono Y, Sounai A, Hori M. Influence of the phosphoric acid-doping level in a polybenzimidazole membrane on the cell performance of high-temperature proton exchange membrane fuel cells. J Power Source 2009;189:943–9.
[27] Jiao K, Li X. Water transport in polymer electrolyte membrane fuel cells. Prog Energy Comb Sci 2011;37:221–91.
[28] Mališ J, Mazúr P, Schauer J, Paidar M, Bouzek K. Polymer-supported 1-butyl-3-methylimidazolium trifluoromethanesulfonate and 1-ethylimidazolium trifluoromethanesulfonate as electrolytes for the high temperature PEM-type fuel cell. Int J Hydrogen Energy 2013;38:4697–704.
[29] Jannelli E, Minutillo M, Perna A. Analyzing microcogeneration systems based on LT-PEMFC and HT-PEMFC by energy balances. Appl Energy 2013; 108:82–91.
[30] Arsalis A, Nielsen MP, Kær SK. Modeling and parametric study of a 1 kWe HT-PEMFC-based residential micro-CHP system. Int J Hydrogen Energy 2011; 36:5010–20.
[31] Zuliani N, Taccani R. Microcogeneration system based on HTPEM fuel cell fueled with natural gas: performance analysis. Appl Energy 2012;97:802–8.
[32] Suzuki A, Oono Y, Williams MC, Miura R, Inaba K, Hatakeyama N, et al. Evaluation for sintering of electrocatalysts and its effect on voltage drops in high-temperature proton exchange membrane fuel cells (HT-PEMFC). Int J Hydrogen Energy 2012;37:18272–89.
[33] Lee J-h, Lee J-H, Choi W, Park K-W, Sun H-Y, Oh J-H. Development of a method to estimate the lifespan of proton exchange membrane fuel cell using electrochemical impedance spectroscopy. J Power Source 2010;195:6001–7.
[34] Araya SS, Andreasen SJ, Kær SK. Experimental characterization of the poisoning effects of methanol-based reformate impurities on a PBI-based high temperature PEM fuel cell. Energy 2012;5:4251–67.
[35] Stevens DA, Dahn JR. Thermal degradation of the support in carbon-supported platinum electrocatalysts for PEM fuel cells. Carbon 2005;43:179–88.
[36] Kim J, Kim M, Kang T, Sohn Y-J, Song T, Choi KH. Degradation modeling and operational optimization for improving the lifetime of high-temperature PEM (proton exchange membrane) fuel cells. Energy 2014;66:41–9.
[37] Kim M, Kang T, Kim J, Sohn Y-J. One-dimensional modeling and analysis for performance degradation of high temperature proton exchange membrane fuel cell using PA doped PBI membrane. Solid State Ionics 2014;262:319–23.
[38] Galbiati S, Baricci A, Casalegno A, Marchesi R. Degradation in phosphoric acid doped polymer fuel cells: a 6000 h parametric investigation. Int J Hydrogen Energy 2013;38:6469–80.
[39] Xu J, Froment GF. Methane steam reforming, methanation and water–gas shift: I. Intrinsic kinetics. AIChE J 1989;35:88–96.
[40] Keiski RL, Salmi T, Niemistö P, Ainassaari J, Pohjola VJ. Stationary and transient kinetics of the high temperature water-gas shift reaction. Appl Catal A: General 1996;137:349–70.
[41] Siegel C, Bandlamudi G, Heinzel A. Systematic characterization of a PBI/H_3PO_4 sol–gel membrane – modeling and simulation. J Power Source 2011; 196:2735–49.
[42] Pisani L. Multi-component gas mixture diffusion through porous media: a 1D analytical solution. Int J Heat Mass Trans 2008;51:650–60.
[43] Poling BE, Prausnitz JM, O'Connell JP. The properties of gases and liquids. McGraw-Hill; 2001.
[44] Liu Z, Wainright JS, Litt MH, Savinell RF. Study of the oxygen reduction reaction (ORR) at Pt interfaced with phosphoric acid doped polybenzimidazole at elevated temperature and low relative humidity. Electrochim Acta 2006; 51:3914–23.
[45] Bergmann A, Gerteisen D, Kurz T. Modelling of CO poisoning and its dynamics in HTPEM fuel cells. Fuel Cell 2010;10:278–87.
[46] He S, Li Y, Wang RZ. Progress of mathematical modeling on ejectors. Renew Sust Energy Rev 2009;13:1760–80.
[47] Fundamentals of heat and mass transfer. 6th ed. Wiley India Pvt. Limited; 2010.
[48] Churchill SW, Bernstein M. A correlating equation for forced convection from gases and liquids to a circular cylinder in crossflow. J Heat Trans 1977; 99:300–6.
[49] Campanari S, Valenti G, Macchi E, Lozza G, Ravidà N. Development of a micro-cogeneration laboratory and testing of a natural gas CHP unit based on PEM fuel cells. Appl Therm Eng. 2014;77:714–20.